PAPER

Gait and locomotion analysis of a soft-hybrid multi-legged modular miniature robot

To cite this article: Nima Mahkam and Onur Özcan 2021 *Bioinspir. Biomim.* **16** 066009

Bioinspiration & Biomimetics

PAPER

Gait and locomotion analysis of a soft-hybrid multi-legged modular miniature robot

Nima Mahkam and Onur Özcan*

Bilkent University, Mechanical Engineering Department, Ankara, Turkey
* Author to whom any correspondence should be addressed.

E-mail: onurozcan@bilkent.edu.tr

RECEIVED
29 March 2021

REVISED
27 July 2021

ACCEPTED FOR PUBLICATION
7 September 2021

PUBLISHED
28 September 2021

Keywords: miniature robots, legged robots, modular robots, robot dynamics, bioinspired robots, gait and locomotion analysis

Supplementary material for this article is available online

Abstract

The locomotion performance of the current legged miniature robots remains inferior compared to even the most simple insects. The inferiority has led researchers to utilize biological principles and control in their designs, often resulting in improved performance and robot capabilities. Additionally, optimizing the locomotion patterns compatible with the robot's limitations (such as the gaits achievable by the robot) improves the performance significantly and results in a robot operating with its maximum capabilities. This paper studies the locomotion characteristics of running/walking *n*-legged modular miniature robots with soft or rigid module connections. The locomotion study is done using the presented dynamic model, and the results are verified using a legged modular miniature robot with soft and rigid backbones (SMoLBot). The optimum foot contact sequences for an *n*-legged robot with different compliance values between the modules are derived using the locomotion analyses and the dynamic and kinematic formulations. Our investigations determine unique optimum foot contact sequences for multi-legged robots with different body compliances and module numbers. Locomotion analyses of a multi-legged robot with different backbones operating with optimum gaits show two main motion characteristics; the rigid robots minimize the number of leg-ground contacts to increase velocity, whereas soft-backbone robots use a lift–jump–fall motion sequence to maximize the translational speeds. These two behaviors are similar between different soft-backbone and rigid-backbone robots; however, the optimal foot contact sequences are different and unpredictable.

1. Introduction

Multi-legged modular miniature robots walk smoother on rough terrains compared to the four-legged robots, which is achieved by performing a variety of statically stable gaits [1, 2]. Furthermore, low weight, versatility, low sensitivity to feet failure, and improved mobility make the multi-legged miniature robots a suitable candidate for accomplishing tasks such as inspection, surveillance, and environment explorations [3]; however, such applications often require gait modification with respect to the walking speed, and terrain characteristics [4]. A common approach to overcome the legged robots' locomotion adaptability problems is to build a reactive system similar to the robots' biological inspirations operating with different pre-planned individually designed gaits. These individually designed gaits are compatible with the new environment and the robot's physical constraints, such as the number of legs and body stiffness, while ensuring the robot's stability.

A modular legged robot shown in figure 1 (SMoLBot) is designed with independent leg actuation and control; therefore the robot is capable of running/crawling with any potential gait. The ability to perform any imaginable gait makes this robot a good candidate to study legged modular robots' locomotion at small-scales. SMoLBot's (figure 1) design incorporates a fabrication method that exploits features of origami-inspired [5–7], soft-hybrid [8] and modular robots [9], at the same time.

This robot represents soft robots' features with the use of polydimethylsiloxane (PDMS) backbones as the connection mechanisms [10]. Modules are cut and folded out of cellulose acetate sheets. Each module is 16.75 mm long, 44.5 mm wide, and 15 mm high, approximately the size of two small-scaled DC motors and a Lipo battery. Similarly, each module is actuated and controlled individually, and the electrical connections between the modules (to synchronize the gait) are made using I^2C pins. A single module consisting of two DC motors, a LiPo battery, an electrical board, and two PDMS locks (where the PDMS backbones are attached) weighs 19 g.

Adapting to terrain variations or operating the robot at its limits (such as the maximum possible speed) is still a challenge for the legged miniature robots. However, it is feasible to overcome this problem using a robot that can operate at different gaits. The gait modification capability makes it feasible to adjust the gait, which is exclusively designed for the robot at a specific stepping frequency. Currently, different approaches exist for gait coordination in multi-legged robots. While large-scaled robots rely on reactive algorithms and contact sensors to sense and react to the environment [11, 12], small-scaled robots tend to operate at a single gait with constant feet phases. That being stated, miniature robots favor the use of commonly known gaits of their biological inspirations (like reptiles, insects, and mammals) such as quadrupeds operating at a walk, trot, pronk, etc [13–16], or hexapods running with an alternating tripod-gait [17, 18] or a wave gait [19]. This different approach of the miniature robots is due to the limitations on the payload capacity, power, and lack of feasible sensors and computational power. However, the efficiency of these commonly known gaits is unknown due to the gait mismatch phenomenon in the legged miniature robots, i.e. the desired-intended gait and the actual gait that the robot is operating with being always different. This gait mismatch is caused by the body orientations (roll, yaw, and pitch angles) changing the feet contact sequence in conjunction with the lack of control on the duration of the feet-ground contact for the miniature robots. Consequently, for a legged miniature robot with independent leg actuation, the robot's dynamics, actual feet contact sequence, design geometry, body compliances, and an overall statically-stable motion should be determined to characterize the optimum gait achieving the miniature robot's full potential. These optimized gaits would satisfy the pre-defined objectives that are considered during the gait design process, such as a maximum translational velocity or a minimum pitch angle, resulting in a robot operating at its limits.

Furthermore, it is essential to note that different design parameters should be considered studying/designing a modular miniature robot and running the robot optimally. Different approaches exist to extend the capabilities of legged modular robots, like using self-reconfigurable robots with magnets [20] to manufacture snake-like mechanisms, or to use active backbones [21] that increase the modular robot's maneuverability. These extra capabilities added to the robot assembly follow up with studies that investigate the effect of the spines' active degree of freedom (DOF) on the effort of grounded reorientation and robot's locomotion [22]. These different approaches can be combined with the work presented here to understand these small-scaled modular robots' dynamics better. Furthermore, while our robot takes advantage of lifting the mid modules by adjusting the front and rear module, such different approaches, like an active spine, can be considered to maximize these small-scaled robots' performance.

While many studies have investigated the locomotion of the legged miniature robots operating with the common know gaits [23–27], a few studies have been conducted on the locomotion of these robots operating at an optimum gait [28, 29]. In this work, we present the locomotion analysis of a multi-legged modular miniature robot. Furthermore, the optimization study presented in this manuscript determines the compatible optimum gaits for an n-legged robot with different backbones, indicating different compliance values between modules. Experimental and simulation results show the existence of different optimum gaits for varying backbone compliances, while the module number is kept constant. Optimum gaits of the n-legged robots defined in this study maximize the robot's translational velocity; however, the same algorithm described in this manuscript can be applied for any other optimization objective. It is important to note that a different optimization-objective can result in a new set of optimized gaits that will possess distinct locomotion behavior (locomotion behavior in this study is defined as the waveform of the roll, yaw, pitch angles, and the position of the robot's center of gravity (COG) at a 3D space in a single gait cycle).

This work's contributions are the gait and the locomotion analysis of an n-legged modular miniature robot with soft or rigid backbones operating with symmetric or asymmetric gaits, analyses proving the existence of unique optimum gaits for different body-compliances of a multi-legged miniature robot, a velocity comparison study determining the unique optimum gaits for the n-legged robots with different body-compliances maximizing the velocity, and locomotion analyses characterizing the key differences between the commonly used gait, such as continuous-trot gait, and the optimum gaits obtained in this study. These results provide a better insight into the dynamics of the multi-legged miniature robots operating with symmetric and asymmetric gaits for researchers working with robots at small-scales. Additionally, by modifying leg kinematics and backbone and module designs, different miniature robots can be

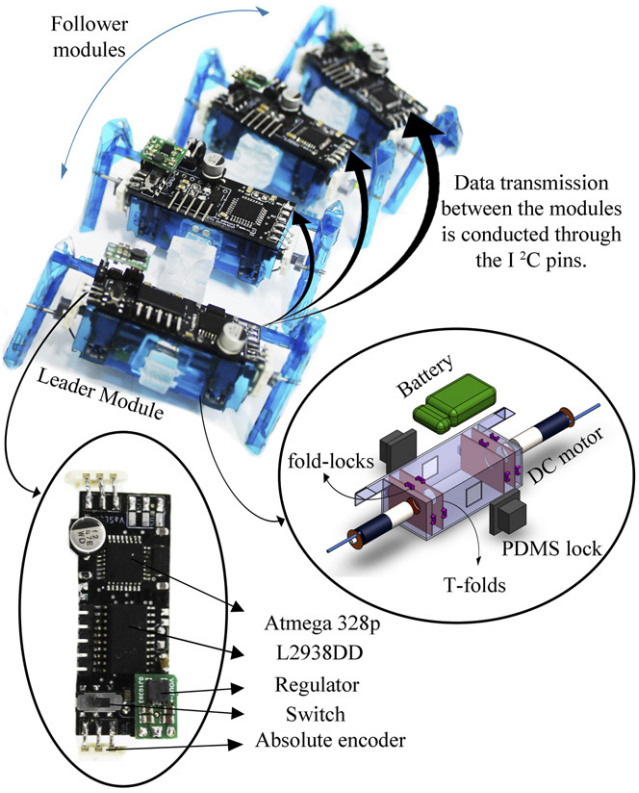

Figure 1. An eight-legged four-module SMoLBot with soft backbones.

analyzed in a similar fashion to identify the optimum gaits for various operational needs.

2. Design and modeling

Design, control strategy, and dynamic model of a multi-legged robot with different backbones stiffnesses are presented in a previous work found in [10, 30]; however, for the sake of completeness of this manuscript, a summary of the robot's design, manufacturing techniques, and the final form of the dynamic formulation are presented here, as well.

2.1. Design and manufacturing–foldable mechanisms, soft structures, and electronics

The modules are manufactured using 100 μm-thick flexible, A4-sized cellulose acetate sheet. Module's assembly consists of transforming a two-dimensional paper sheet to a complex three-dimensional structure with subsequent folding of the acetate sheets [10, 31]. Optimized fold-locks and parallel T-folds used in the modules result in a highly resilient assembly that removes the twist and buckling movement of the body. A combination of the fold-locks and the T-folds hold two DC motors (Pololu, sub-micro plastic planetary gear motor) and a single cell 3.7 V, 150 mAh Li–Po battery inside each module. Two PDMS locks embedded in each module are placed on the front and the rear patches using tight-fit rectangular holes. An eight-legged four-module SMoLBot and its electrical components are shown in figure 1.

Figure 2 shows the folding procedure of a foldable leg. The legs are four-bar linkages with a single DOF. Each leg is connected to the main body through a single DOF rotational 3D printed cam-shaft and fold-locks. The 3D printed cam-shaft constructs a tight-fit connection between the DC motor and the leg. Triangular beam parts of the folded leg are the rigid links, and thin-plates connecting the triangular beams act as compliant joints. Leg dimensions are calculated using the four-bar linkages' design techniques, considering a relatively long stride length and large foot lift for better walking.

2.2. Dynamic model

A comprehensive dynamic model of an n-legged miniature robot with soft or rigid backbones is obtained using Newton–Euler formulation and is presented in [30]. The dynamic model is dependent on the physical properties of the contact and the constant backbone parameters, such as lengths, stiffness values, etc. Backbones in the dynamic model are modeled as rotational springs and dampers that connect two individual modules. The dynamic model predicts the locomotion behavior of the robot, by estimating the position, the orientation, and rate of change of position and orientation for the robot's COG and the modules' COG. Dynamic model parameters are expressed in different coordinate systems as shown in figure 3: a fixed inertial reference frame attached on the ground (C_I), a coordinate system that is attached to the instant position of robot's COG (C_{CG}), and N

Figure 2. Step-wise leg folding process.

coordinate systems that are attached on the modules' COG (C_{Mi}), where i donates the module number ($i = [1, 2, \ldots, N]$). Equations (1)–(6) define the dynamics of an n-legged robot with soft or rigid body in a three-dimensional space.

$$\dot{V}_{CG} = \frac{F_{CG}}{m} - \Omega_{CG} \times (MV_{CG}) \tag{1}$$

$$\dot{\Omega}_{CG} = I_G^{-1}(M_{CG} - \Omega_{CG} \times (I_G\Omega_{CG}) - \dot{I}_G\Omega_{CG}) \tag{2}$$

$$\dot{R}^I_{CG} = H^I_i \begin{bmatrix} u \\ v \\ w \end{bmatrix} \tag{3}$$

$$\dot{\Theta}^I_{CG} = L^I_i \begin{bmatrix} p \\ q \\ r \end{bmatrix} \tag{4}$$

$$\dot{\Omega}^i_{CG} = (I_{Mi})^{-1}(M^i_{CG} + \kappa^{i-1}\delta\varphi^i_F - \beta^i - \delta\varpi^i_F + \kappa^i\delta\varphi^i_B - \beta^i\delta\varpi^i_B + I_{Mi}\alpha^{Mi}_{CG} - \Omega^i \times (I_{Mi}\Omega^i)) \tag{5}$$

$$\dot{\Theta}^I_i = L^I_i \begin{bmatrix} p_i \\ q_i \\ r_i \end{bmatrix}. \tag{6}$$

In equations (1)–(6), R^I_{CG}, $V_{CG} = [u, v, w]^{\mathrm{T}}$, $\Theta^I_{CG} = [\phi^I_{CG}, \theta^I_{CG}, \psi^I_{CG}]^{\mathrm{T}}$, $\Omega_{CG} = [p, q, r]^{\mathrm{T}}$ are the position, the rate of change of position defined for the robot's COG and angular orientation (in the form of Euler angles) and their time rate change, respectively. $\Theta^I_i = [\phi^I_i, \theta^I_i, \psi^I_i]^{\mathrm{T}}$, $\Omega^i_{CG} = [p_i, q_i, r_i]^{\mathrm{T}}$ are the orientation vector and the rate of change of the orientation vector for each module. F_{CG} and M_{CG} are the forces and the moments acting on the robot's COG. M^I_{CG} shows the moments acting on each module with respect to the reference frame attached on the C_{Mi}. M and I_G are the constant mass and moment of inertia of the robot, and I_{Mi} is the moment of inertia of a single module. M^i_{ext} are the external moments due to the backbones. Ω^i is the vector sum of Ω^i_{CG} and Ω_{CG}, expressed in C_i. α^{Ci}_{CG} is the angular acceleration of the robot's COG represented in the reference frame attached to the ith module (C_i). H^I_i and L^I_i are the transformation matrices represented in the form of Euler angles [32].

Dynamic representation in (1)–(6) define the 12 states of the robot's COG and $6 \times (N-1)$ states of the modules, given by:

$$\chi = \left[R^I_{CG}, V_{CG}, \Theta^I_{CG}, \Omega_{CG}, \Theta^I_2, \Omega^2_{CG}, \ldots, \Theta^I_N, \Omega^N_{CG}\right]^{\mathrm{T}}.$$

$\dot{\chi}$ determines the locomotion of the robot's and the modules' COGs. For any given initial condition, MATLAB's numerical stiff solver ode15*s* is used to solve the system of ODEs in (1)–(6).

The presented gaits in this study (section 4) are determined directly from the dynamic model. Next, these gaits are verified with our modular robot operating with similar gaits (please refer the supplementary video (https://stacks.iop.org/BB/16/066009/mmedia) attachment that shows the actual robot running with optimum gaits and their comparison with the simulations). Predicting unknown asymmetric gaits and their agreement with the actual robot shows the fidelity of the presented dynamic model and the algorithm. The model can predict uncommon locomotion trends with random gaits that have not yet been investigated in modular robotic platforms with compliant backbones. This shows the possibility of using the dynamic model and presented formulations for any other modular robot with compliant backbones; however, adjustments are required to match the physical properties of the simulated robot similar to the actual robot.

3. Optimization algorithm

The optimization study presented in this manuscript investigates a large number of possible gaits in the gait-space of an n-legged robot with soft and rigid backbones to maximize the robot's translational

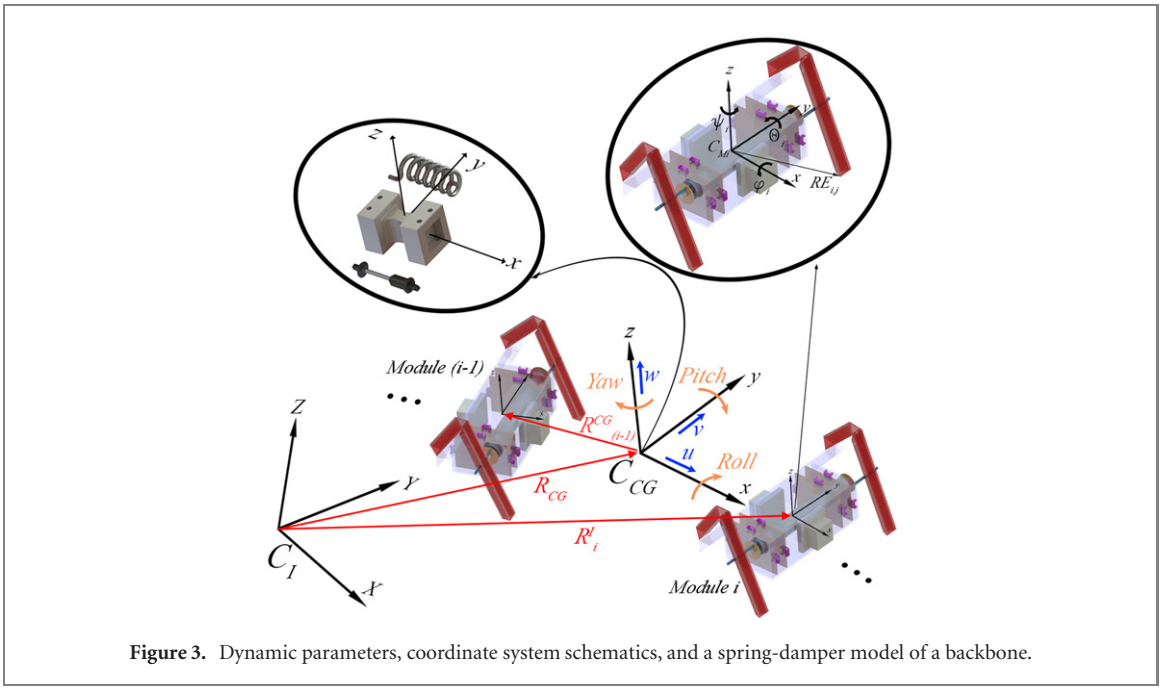

Figure 3. Dynamic parameters, coordinate system schematics, and a spring-damper model of a backbone.

velocity. Additionally, in the case of a different optimization goal rather than the translational velocity, the optimum gaits could be different; however, the same procedure mentioned in this section can be utilized to obtain the optimum gaits with the new objective.

A vast growing literature studies the large-scale robots' locomotion behavior. Numerous studies investigate trajectory optimization algorithms using rigid body dynamics combined with penalty-based optimization methods [33] and multi-contact mechanics with complementarity constraints [34, 35] to further enhance these large rigid robots' capabilities. The main differences between our study and these types of trajectory optimization investigations for larger robots are the system's DOF, limited computational power and sensors at miniature-scale, and the foremost objective of the research. The minimum DOF of our modular robot is 18 (usually 8 to 13 for large-scale rigid robots) that corresponds to 18 coupled non-linear ODEs (up to 42 ODEs, particularly for the study in this research), which makes the entire system computationally heavy. Designing a miniature robot with specific design parameters based on a preliminary optimization study is essential for these small-scale robots. This is due to the lack of computational power and limited sensors that constraints the use of live optimization techniques and complicated control algorithms on the actual miniature robot. This manuscript shows how running a multi-legged robot with a unique gait improves the robot's performance and the importance of these analyses before deploying these miniature modular robots, without touch and force sensors, in a real-world environment. For our study case, GA is chosen to determine the feet phases corresponding to the optimum gait. The nature of GA looks for the best set of parameters in a population of points rather than a single point, albeit not guaranteeing any optimality. Even though the optimality is somewhat compromised, checking multiple operating points simultaneously helps to examine different locally optimum gaits and understand their characteristics. Additionally, implementing GA does not require the derivatives of the objective function, making the optimization algorithm's implementation to the dynamic model straightforward. The approach mentioned in the following paragraph and GA satisfy this research's needs and make it possible to understand the dynamics at a small scale and characterize many previously unknown locomotion behaviors.

Gaits are motions of the feet that define the contact sequence of each foot in a periodical sequence. In this study, $(n-1)$ unique phases, where n shows the number of feet, is selected to define the gait; i.e. since the gait is a periodical motion, the origin of the absolute phase is arbitrary and is considered to be the phase of the leg R_1 (right foot of the leader module, module $N = 1$). For the robot's single leg shown in figure 4 and its generalized four-bar model, $BD = 3$ mm, $CD = 16.18$ mm, $AC = 16.83$ mm, and $DE = 21.86$ mm. Additionally, the leg naming pattern used in this study is shown in figure 5.

The rotation angle $(\theta^{i,j})$ of the link BD for the leg j of the module i, defined about the negative Y axis of the C_{Mi}, is derived from the relationship between the joint's constant stepping frequency and its phase as follows;

$$\theta^{i,j} = \omega^{i,j} t + \phi^{i,j}, \tag{7}$$

where, $\phi^{i,j}$ shows the foot phase based on the origin of the absolute phase and t is the time. Additionally, to determine the optimum gait of an n-legged robot with a constant stepping frequency and different types

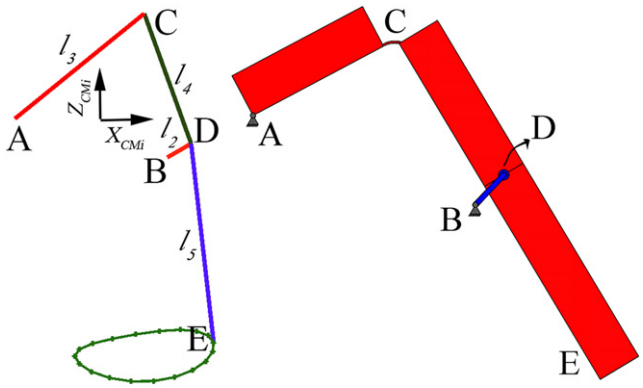

Figure 4. Four-bar leg schematic showing the locations of the corresponding labels of a folded leg.

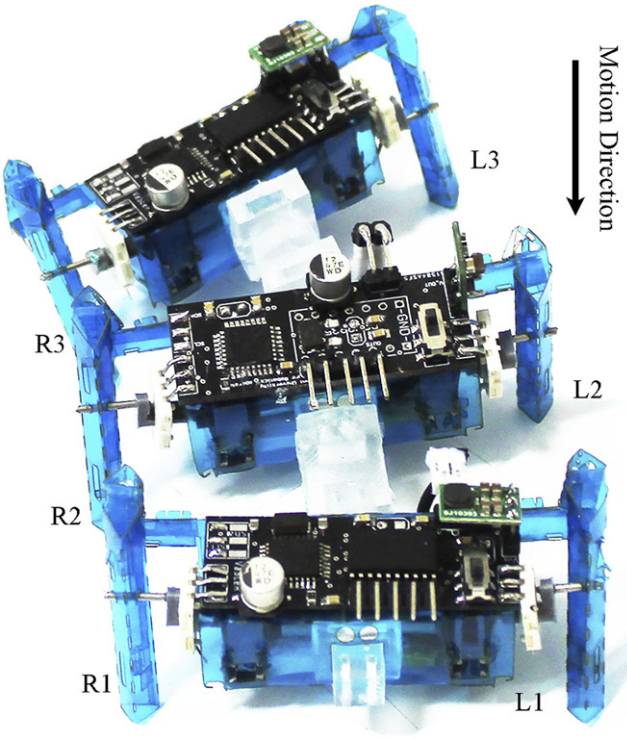

Figure 5. The feet naming pattern used in this study.

of backbones, the performance index R is defined as:

$$P_m = \sqrt{(x_{m+1} - x_m)^2 + (y_{m+1} - y_m)^2}, \quad (8)$$

$$D_m = P_m . \text{sign}(u^m), \quad (9)$$

$$V = \frac{\sum_{m=1}^{ST-1} D_m}{t_{\text{end}} - t_1}, \quad (10)$$

$$R = \frac{V_{\max}}{V}, \quad (11)$$

where t_1 shows the transient motion's finishing instant, robot possessing a stable periodical motion. ST is the number of time steps of the simulation starting from $t = t_1$ to $t = t_{\text{end}}$. x and y show the COG position in inertial reference frame C_I, and P_m is the COG position vector's magnitude at each time step. u^m is the COG's translational velocity along the x axis of the body attached frame as defined in equation (6). $\text{sign}(u^m)$ shows the instantaneous movement direction, where $\text{sign}(u^m) = +1$ is used for striding and $\text{sign}(u^m) = -1$ for the sliding motion of the robot. D_m and V indicate the instantaneous position vector and the robot's overall translational velocity, respectively. $V_{\max}$ is the temporary maximum velocity.

The gait optimization study at a constant stepping frequency f is implemented using genetic algorithm optimization by minimizing the R value. Genetic algorithm is chosen considering the unpredictable behavior of the objective function (velocity of the robot operating with an unknown gait) that introduces multiple locally optimal solutions to the system and inherently parallel characteristics of the GA that seek multiple possible optimum gait candidates as the

optimum solution. Additionally, since GA can handle the large and wide solution space [36] of the possible gaits existing in this study, it appears to be a nice candidate for this problem. It should be pointed out that the phrase 'unpredictable behavior of the objective function' refers to the high dependency of the velocity on many different design parameters such as the gait. Unlike quadrupeds, in many-legged robots, minor changes in the gait (like switching the feet phases of the modules), or any other design parameter, significantly changes the robot's locomotion behavior. As an example, changing the feet phases of the front and rear legs in a four-legged robot operating with any commonly known gait (such as trot, walk, canter, etc.) does not affect the running velocity. However, a similar change in a six-legged robot (where the feet phases of two modules are switched) can reduce/increase the velocity up to 30%–40% of the original velocity. Furthermore, examining the effect of the stepping frequency, body compliances, and the number of legs, in addition to the operating gait, makes locomotion analyses of the miniature robots even more complicated.

With the aim of obtaining all possible gaits that maximize the robot's velocity and avoiding sets of feet phases that result in a turning robot, a secondary correction algorithm is integrated within the optimization code. Secondary correction algorithm considers a correction parameter C that is defined as equation (14).

$$u_1^I = H_{CG}^I u_1, \quad \text{at} \quad t = t_1, \tag{12}$$

$$u_2^I = H_{CG}^I u_2, \quad \text{at} \quad t = t_2, \tag{13}$$

$$C = \sin^{-1}\left(\frac{u_1^I \times u_2^I}{|u_1^I||u_2^I|}\right), \tag{14}$$

where, $t_2 - t_1 = 1$ s. u_1 and u_2 show the robot's instantaneous velocity vector at $t = t_1$ and $t = t_2$ along the robot's length represented in C_I reference frame, respectively. C defines the angle between u_1^I and u_2^I, and measures the amount of deviation angle in $t_2 - t_1$.

Genetic algorithm optimization, in conjunction with the secondary correction algorithm, investigate the feasible gait space of the miniature robot to maximize the robot's velocity, while the stepping frequencies of the feet are equal and constant, as follows;

- A set of initial population is defined by the GA.
- A set of optimization parameters (OP) is selected.
- Locomotion of the robot with selected OP is analyzed.
- Performance index R is determined.
- Performance index C is determined.
- If $C >= 10^\circ$ then $R = \infty$.
- If $R <= 1$ then

$$V_{\max} = \frac{\sum_{m=1}^{ST-1} P_m.\,\text{sign}(u^m)}{t_{\text{end}} - t_1},$$

$$\text{OP}_{\text{best}} = \text{OP}.$$

- $V_{\max}$ and OP_{best} are updated.
- Iteration continues until the iteration limit or the maximum time is achieved.

The algorithm mentioned above provides an optimum gait and local optimal results tested during the optimization process.

The locomotion study compares the multi-legged robot's motion operating with a commonly known gait such as the trot gait and the optimum gait. This locomotion study provides a better insight into the multi-legged robot's locomotion behavior while running with different, unfamiliar, and asymmetrical gaits at small-scales. As stated earlier, the term 'locomotion behavior' throughout this manuscript refers to the COG motion in the XZ plane and the roll, pitch, and yaw angles of the robot's COG, i.e. these four variables are the main parameters that define the characteristics of the overall motion of the robot. Additionally, this optimization study is done iteratively with different initial populations to initialize the GA algorithm. The initial population of each trial is chosen using the local optimum results found in the previous trials. Discussion on the locomotion behavior of a multi-legged robot with different backbone types while operating with the optimum gaits are presented in the next section.

4. Numerical and experimental results

The miniature robots' locomotion study shows a significant difference between the intended gait and the robot's actual walking/running gait. This gait mismatch is mainly because of the rigid body dynamics and the uncontrolled contact duration of the feet that results in a different contact sequence compared to the contact sequence of the intended gait, e.g. figure 6(a) shows the intended gait (trot gait where two side-by-side legs are 180° apart in-phase and the diagonal legs of the two consecutive modules are in phase) and the actual gait of the four-legged two-module robot. A four-legged robot operating with a trot gait is supposed to stride on two periodically changing diagonal feet (figure 6(a)-green); but the robot often falls on a third leg forming a tripod (figure 6(a)-blue). The formation of the tripod results in a motion where the rear legs are dragged on the ground. This dragging motion introduces an undesired friction force decreasing the robot's translational velocity. Furthermore, leg slip is another main detrimental factor of the locomotion speed at the miniature scale. Slip decreases the stride length, and the dragging forces decrease the net effective force pushing the robot forward. Figure 6(b) shows the slip and the stride length definitions in a single foot trajectory. The gait mismatch and the foot slip are two main reasons to investigate an optimum gait for an n-legged miniature robot using a full model

Table 1. Backbone stiffness values.

Stiffness (mN.m Rad^{-1})	Rigid	Comp.(T)	Comp.(I)
k_t	∞	200	15
k_{b1}	∞	470	130
k_{b2}	∞	470	30

of robot's dynamics. The gait optimization study presented in this manuscript considers the robot's actual gait and dynamics of the soft and rigid bodies in order to eliminate/decrease the feet drag and the feet slip to maximize the robot's velocity.

Using the optimization procedure outlined in section 3 a numerical study on the gaits of the robot with different backbone types at 3 Hz stepping frequency is implemented. Three types of backbones are used in experiments: rigid, only-torsional, and I-shaped compliant backbones. Rigid backbones are PDMS blocks with metal insertions that possess the highest bending and torsional stiffness. Torsionally compliant backbones are rectangular-shaped PDMS beams with a single DOF (rotation around the central axis of the backbone), and I-shaped complaint backbones possess relatively the lowest bending and torsional stiffnesses with multiple DOF (figure 7). Throughout the manuscript, the torsionally compliant and I-shaped complaint backbones will be referred as compliant(T) and compliant(I), respectively. Table 1 shows the stiffness values of the backbones, where k_t, k_{b1} and k_{b2} are the torsional stiffness and the bending stiffnesses along with the width (k_{b1}) and height (k_{b2}) of the backbone, respectively. Stiffnesses values of the backbones are derived using beam bending and torsional stiffness formulations according to [37], and the stiffness values of the rigid backbones are assumed to be infinity.

Generally, gaits are classified as walks or runs. The distinction is made based on the duty cycles of the feet. For example, the walk gait for quadrupeds is defined where the duty cycles of the feet are higher than 0.5, which indicates a stage where at least three legs are in contact with the ground at the same time. Gaits are also classified as symmetrical and asymmetrical [23]. A symmetrical gait is a type of motion pattern in which the adjacent right and left legs have an equal duty cycle (and usually equal to 0.5), such as the common gait for the hexapods known as alternating-tripod gait. This gait uses the same foot phase identification as the biologically-inspired trot gait, where each foot has a 0.5 duty cycle, and the adjacent rear-front and right-left feet are 180° apart in phase. Similarly, we use the same symmetrical gait generation method to determine the foot phases for the robots with more legs. For an n-legged robot, the feet phases of the odd-numbered modules are similar to the first module (leader), and the feet phases of the even-numbered modules are the same as the second module of the robot. This gait generation method produces a symmetrical gait, where individual right and left feet have 180° phase difference. This symmetric gait is the generic gait used in the legged robots called alternating-tripod gait for six-legged robots, and we call it continuous-trot gait for robots with more legs. Using the optimization study presented here, we are trying to improve these symmetric gaits.

An investigation to find the optimum gaits improving the robot's performance and velocity is conducted. First, the dynamic model and the proposed optimization algorithm are used to determine the optimum foot phases for an n-legged modular miniature robot with soft or rigid backbones. Next, the optimum gaits are verified using a soft-bodied legged modular miniature robot running at different stepping frequencies. The velocities of the simulated robot shown in figures 8, 11 and 14 are determined in the range of 0–4 Hz to inspect the legged modular miniature robot's locomotion in a wider stepping frequency domain; then the results are verified using a legged miniature modular robot operating with the optimum gait at 2 and 3 Hz and the continuous-trot gait between 1 to 4 Hz stepping frequencies. Figure 8 shows the velocity results of the six-legged three-module robots operating with the alternating-tripod gait and the optimum$_3$ gait (optimum gait obtained at 3 Hz stepping frequency). Experimental velocity results shown in figure 8 match with the simulation results up to a considerable degree. The maximum error (e), defined as the relative difference between the V_{sim} and V_{exp}, in figure 8 is 13 mm(s)$^{-1}$ that is less than 0.11 body-length/s.

The lack of feasible small-scaled sensors and limited computational power restricts the use of complicated control algorithms based on force/touch sensors in the miniature scale. Due to similar constraints and unavailability of the touch sensors, the presented gaits are verified by comparing the velocity of an actual robot operating at the desired gait and the simulated one. The velocity results presented in this study are in good agreement with experiments that show the model's accuracy in estimating different locomotion trends of a modular robot with various body stiffnesses. Additionally, the dynamic model and the formulation predicting the locomotion trends of a multi-legged robot with different body compliances are verified with many other dynamic parameters, such as roll and pitch angles, found in [30]. Additionally, it is necessary to note that the optimum gaits in this study are obtained at 3 Hz stepping frequency, and the experimental results of the robot operating with these optimum gaits are presented at 2 and 3 Hz stepping frequencies to validate the numerical study. Additionally, the robot's locomotion behavior is studied in the range of 0 to 4 Hz, which is the achievable and controllable frequency range of the actuators. In other words, the optimum gait results presented in this study are only optimum at 3 Hz stepping

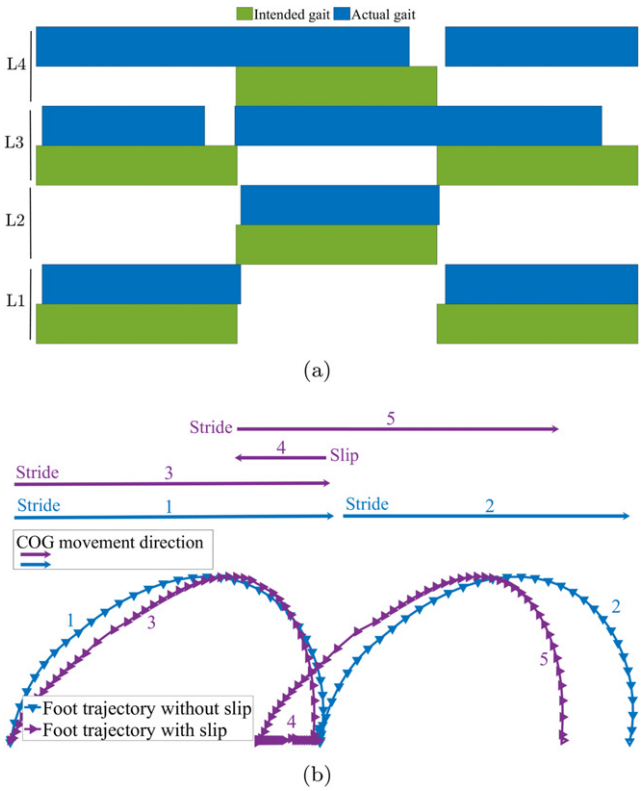

Figure 6. (a) Gait diagram of a four-legged two-module robot operating with a trot gait, the color regions indicate feet-ground contact (the actual and the intended gait). (b) Trajectories of the robot's foot in the presence and the absence of the slip motion and the COG's movement direction in a single gait cycle.

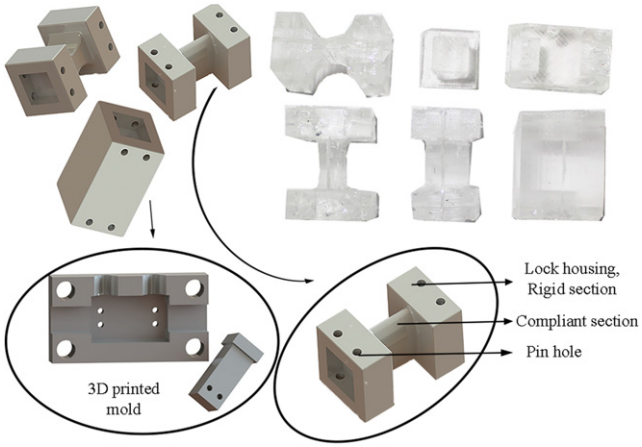

Figure 7. PDMS backbones and a PDMS lock used in the robot assembly.

frequency. The optimization would result in different optimum gaits for each stepping frequency value. Since, this means an infinite number of optimum gaits, one stepping frequency and one optimum gait is chosen to generate the results and make the study feasible.

The optimization study of the six-legged robots shows a noticeable increase in the velocity values of the robot with compliant(I) backbones (figure 8-blue lines), i.e. **robot with compliant(I) backbones possesses the relatively highest velocity deviation while operating with the optimum$_3$ gait compared to the same robot operating with the continuous-trot gait**, e.g. for the six-legged three-module robot with compliant(I) backbones the velocity increased from $V_{\text{trot}} = 50$ mm(s)$^{-1}$ to $V_{\text{opt}} = 80$ mm(s)$^{-1}$ which gives $\delta V = 30$ mm(s)$^{-1}$, while δV for the robots with rigid and compliant (T) backbones are approximately 15 mm(s)$^{-1}$ and 10 mm(s)$^{-1}$, respectively.

Table 2 shows the optimum$_3$ feet phases of the six-legged three-module robots, where the compliance between the modules ranges from rigid to soft.

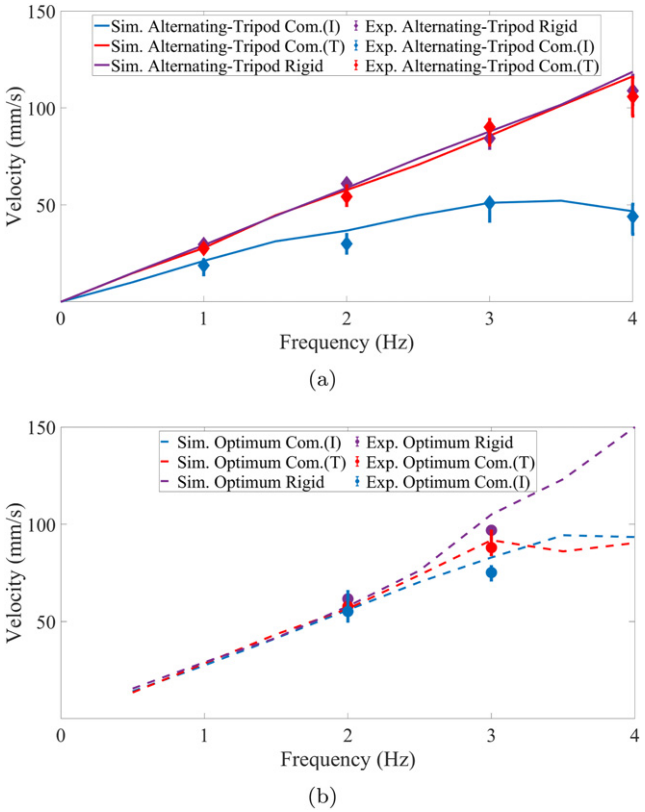

Figure 8. Simulation and experimental velocity results of the six-legged three-module robots with rigid, compliant(T) and compliant(I) backbones operating with (a) alternating-tripod gait, and (b) optimum$_3$ gait.

Table 2. Motor phases of the six-legged three-module robot for optimum$_3$ gait.

	SMoLBot(I)	SMoLBot(T)	SMoLBot(R)
$R_1 - L_1$(deg)	0–155	0–26	0–170
$R_2 - L_2$(deg)	5–18	170–174	67–180
$R_3 - L_3$(deg)	155–167	10–10	180–17

The SMoLBot(R), SMoLBot(T), and SMoLBot(I) used in the text are the short forms of multi-legged robots with rigid, compliant(T) and compliant(I) backbones, respectively. The optimum feet phases for the rigid case is close to the alternating-tripod gait, whereas the feet phases for the compliant backbone robots are significantly different from generic alternating-tripod gait. Figures 9 and 10 illustrate the robot's actual gait diagram and the locomotion behavior with compliant(I), compliant(T), and rigid backbones in a single gait cycle.

Figures 9(a) and (c) show the feet contact sequence of Robot(I) operating with the optimum$_3$ gait and the alternating-tripod gait, respectively. Legs on Robot(I) operating with the continuous-symmetrical form of the trot gait (alternating-tripod gait) have zero lift, and the robot tends to crawl on the ground (figure 9(b)-blue showing the COG motion in a single gait cycle). However, SMoLBot(I) operating with the optimum$_3$ gait tends to bounce rather than crawl (figure 9(b)-red), where each module is lifted in a periodical sequence. This is also shown in the results presented in table 2. **A six-legged robot with compliant(I) backbones operating with the optimum$_3$ gait has a jump and fall locomotion pattern where the rear legs are almost always on the ground to form a support for the robot to jump (L_3 and R_3 in figure 9(a)).** Roll and pitch angles of the six-legged three-module robot with alternating-tripod gait and the optimum$_3$ gait are shown in figure 9(d). As discussed earlier, six-legged robot with compliant(I) backbones uses the rear module legs as the support to jump, the mid-module to lift and stride, and the front module to stride. Similarly, this motion behavior is seen in the pitch angle of the six-legged three-module robot operating with the optimum$_3$ gait (figure 9(d)-red). The increasing pitch is the lift part of the motion, and the decreasing pitch is the second module's stride period. Furthermore, since the differences between two side-by-side feet phases for the optimum gait are lower compared to the alternating-tripod gait (where the side-by-side feet are 180° apart in-phase and maximum), the SMoLBot(I) operating with the optimum$_3$ gait has a lower roll angle compared to SMoLBot(I) operating with the alternating-tripod gait (figure 9(d)-magenta).

Figures 10(a) and (c) show the optimum$_3$ gait diagrams of the six-legged three-module robot with compliant(T) and rigid backbones, respectively. **Similar to SMoLBot(I), the six-legged three-module**

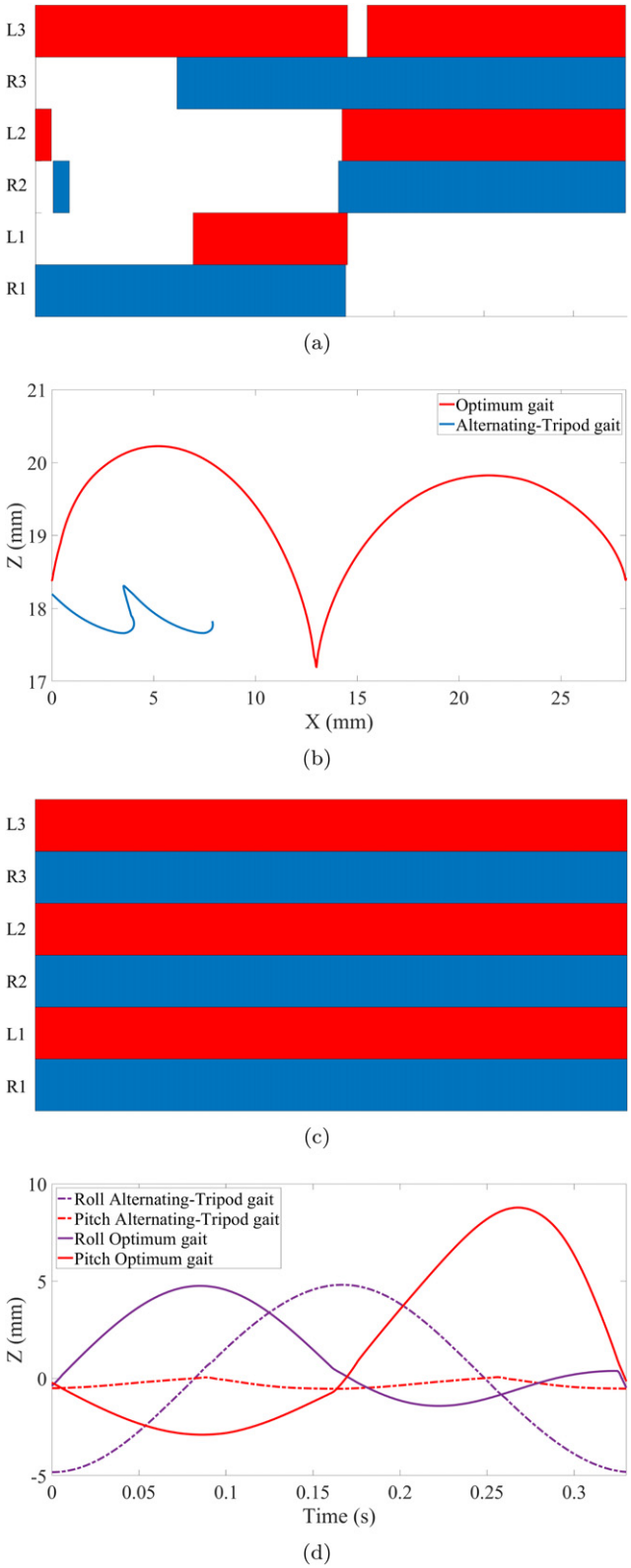

Figure 9. (a) Optimum$_3$ gait diagram of the six-legged three-module robot with compliant(I) backbones. (b) The six-legged three-module robot's COG in a single gait cycle. (c) Gait diagram of the six-legged three-module robot with compliant(I) backbones operating with the alternating-tripod gait. (d) Roll and pitch angles of the six-legged three-module robot with compliant(I) backbones operating with alternating-tripod and the optimum$_3$ gait in a single gait cycle.

SMoLBot(T) operating with the optimum$_3$ gait has a bouncy motion that lifts and drops the front modules. However, the six-legged robot with rigid backbones tends to use a different contact sequence such that, during a full cycle of the gait, only two legs are in contact with the ground, which follows with a fall on the third leg. Figures 10(b) and (d) show the roll and pitch angles of SMoLBot(T)

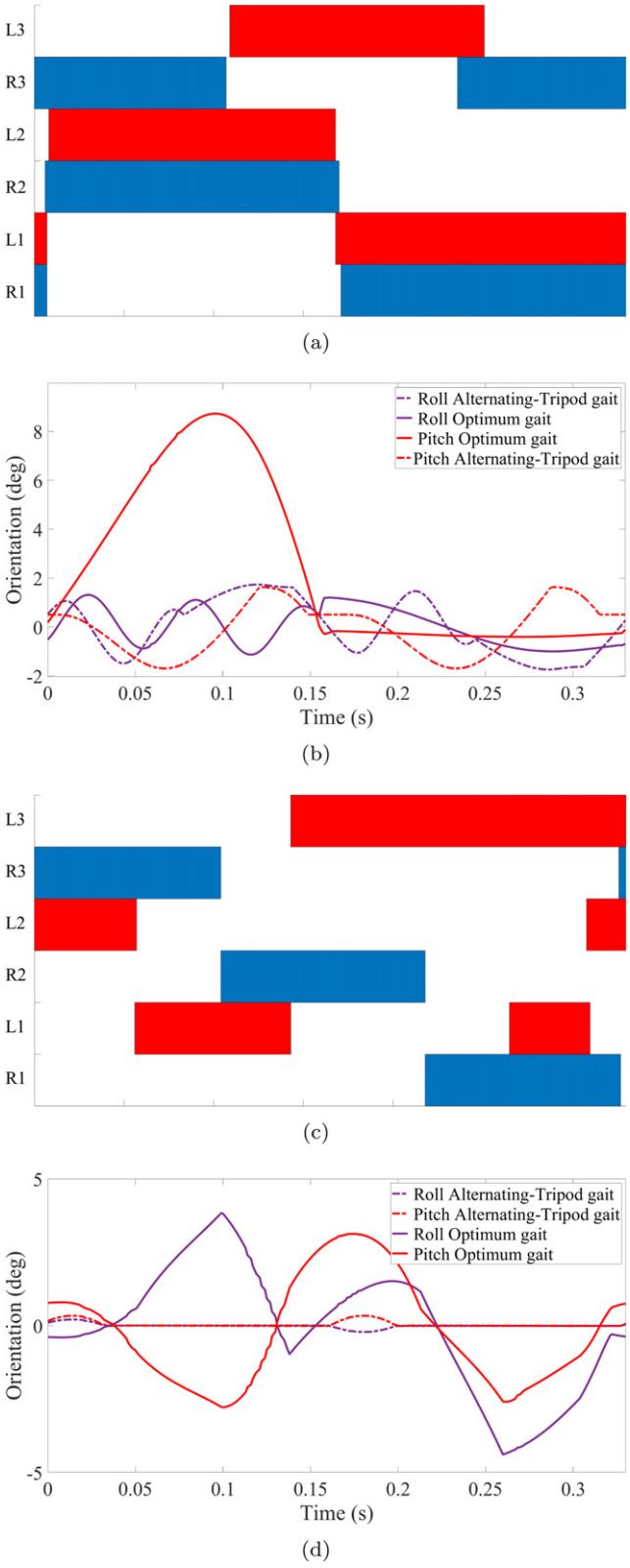

Figure 10. (a) Optimum$_3$ gait diagram of the six-legged three-module robot with compliant(T) backbones. (b) SMoLBot(T)'s roll and pitch angles operating with the alternating tripod and the optimum$_3$ gait in a single gait cycle. (c) Optimum$_3$ gait of the six-legged three-module robot with rigid backbones. (d) Robot's roll and pitch angles with rigid backbones running with the alternating tripod and the optimum$_3$ gait in a single gait cycle. One full stepping cycle is shown in (a)–(d).

and SMoLBot(R) operating with alternating-tripod and optimum$_3$ gait, respectively. The robot's gait and locomotion behavior with only-torsional backbones operating with the optimum$_3$ gait is almost similar to robot with compliant(I) backbones. Similar to the SMoLBot(I), the lift and the drop motion of the SMoLBot(T) can be seen in pitch angle (shown in figure 10(b)-red; however, SMoLBot(T) rolls less

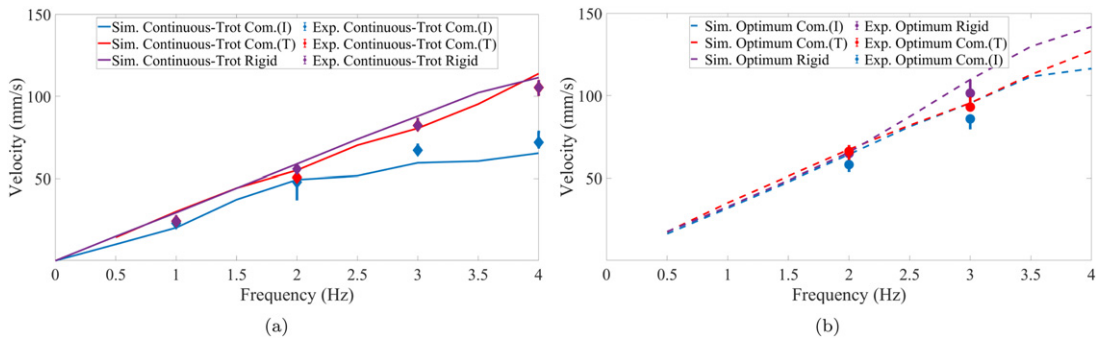

Figure 11. (a) Simulation and experimental velocity results of the eight-legged four-module robots with rigid, compliant(T) and compliant(I) backbones operating with (a) continuous-trot gait, and (b) optimum$_3$ gait.

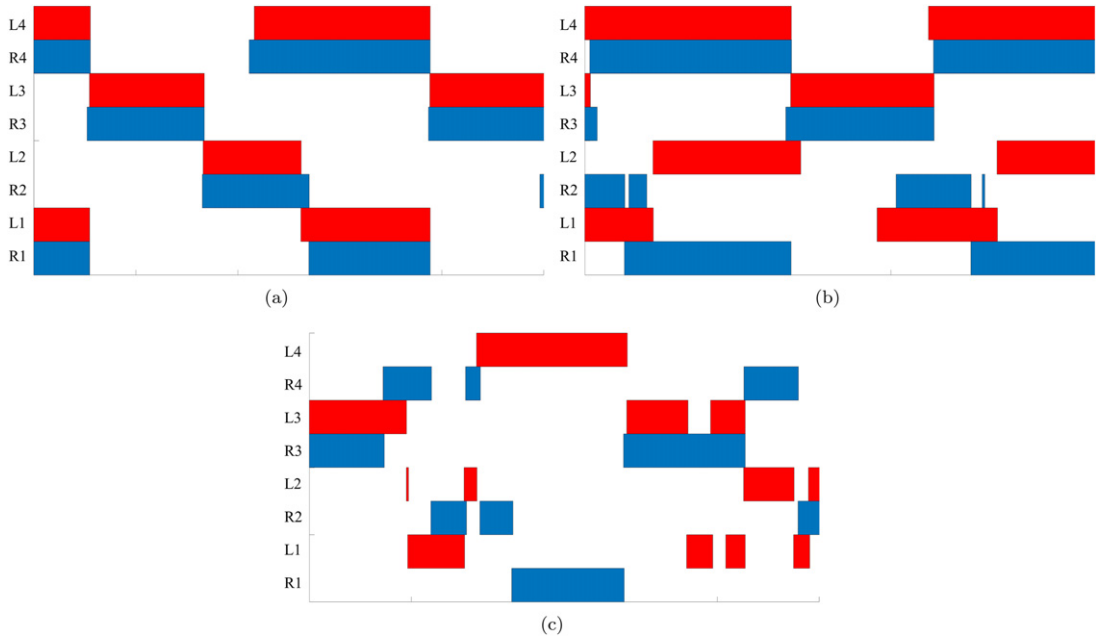

Figure 12. Optimum$_3$ gait diagram of the eight-legged four-module robots in a single gait cycle with (a) compliant(I), (b) compliant(T), and (c) rigid backbones.

than SMoLBot(I) (figures 10(b) and 9(d) magenta lines). In brief, the compliant(T) backbone's higher torsional stiffness compared to the compliant(I) backbone limits the DOF of each module and decreases the roll angle range. The six-legged three-module robot with rigid backbones operating with the alternating-tripod gait has almost zero roll and pitch angles. These low values of pitch angle can be explained considering the statically stable behavior of the continuous form of the trot gait; at least three diagonal feet of the robot are always in contact with the ground resulting in negligible roll and pitch angles. **However, the rigid-backbone robot operating with optimum$_3$ gait possesses considerable roll and pitch angles, and the pitch angle has a periodically changing positive–negative behavior indicating a locomotion type where the front and rear of the robot are lifted periodically.**

Figure 11 shows the velocities of the eight-legged four-module robots operating with the optimum$_3$ gait and the continuous-symmetrical form of the trot gait. Similar to the six-legged robot, the eight-legged four-module robot with compliant(I) backbones possesses the highest velocity deviation between the optimum and the continuous-trot gait. The robot's translational velocity is increased from $V_{\text{trot}} = 60\,\text{mm(s)}^{-1}$ to $V_{\text{opt}} = 90\,\text{mm(s)}^{-1}$ which gives $\delta V = 30\,\text{mm(s)}^{-1}$. Additionally, δV for the eight-legged robots with rigid and compliant(T) backbones are approximately $20\,\text{mm(s)}^{-1}$ and $15\,\text{mm(s)}^{-1}$, respectively. Maximum relative error among all the results (between the simulations and the experiments) in figure 11 is at 4 Hz for the robot with compliant(T) backbones, where e is approximately $10\,\text{mm(s)}^{-1}$ and 0.1 body-length/s.

Table 3 shows the optimum$_3$ feet phases of the eight-legged four-module robots with compliant(I), compliant(T), and rigid backbones. Optimum$_3$ actual

Table 3. Motor phases of the eight-legged four-module robot for optimum$_3$ gait.

	SMoLBot(I)	SMoLBot(T)	SMoLBot(R)
$R_1 - L_1$(deg)	0–0	0–172	0–132
$R_2 - L_2$(deg)	62–90	155–0	32–118
$R_3 - L_3$(deg)	162–173	180–180	180–180
$R_4 - L_4$(deg)	77–50	80–108	100–15

gait diagrams of the robots with compliant(I), compliant(T), and rigid backbones are shown in figure 12. **Results in table 3 and figure 12 show that the optimum gaits for all robots move the legs of the 3rd module at the same phase resulting in bouncing of this module. Moreover, the compliant backbone robots repeat this behavior for the 4th module as well. Additionally, the bouncing of the 3rd and the 4th modules are complementary, i.e. when the 3rd module bounces up, the 4th module touches the ground and vice versa.**

The feet trajectories of SMoLBot(R), SMoLBot(T), and SMoLBot(I) are shown in figure 13, which demonstrate the locomotion behavior of the robot in a single gait cycle, where $Z = 0$ indicates the contact between the foot and the ground. Figure 13(a) shows the feet trajectories and the feet contact sequence for the robots with compliant(I) backbones operating with optimum$_3$ gait. Eight-legged four-module SMoLBot(I) operating with the optimum$_3$ gait follows a contact sequence such that, in a large portion of the gait cycle, only two periodically-changing feet are in contact with the ground (figure 12(a)). The optimum gait decreases the effect of the undesired leg slip, which is the main reason for not achieving the maximum velocity possible in small-scaled robots [38, 39], i.e. no-slip motion is observed for the feet of the second and the third modules (figure 13(a)), however, the first module and the last module slip in a single gait cycle that is caused by the DOF of the compliant(I) backbones. The slip-lengths for modules $N = 1$ and $N = 4$ are less than 3 mm. The robot's COG, while operating with the optimum$_3$ gait, possesses a much lower slip-length compared to the $N = 1$ and $N = 4$ modules since the COG is approximately located between the second and third module, where no slip motion is observed.

Figures 12(b) and 13(b) show the optimum$_3$ gait diagram and the feet contact sequence of the eight-legged four-module robot with compliant(T) backbones. A previous study found in [30] shows that robots with compliant(T) backbones suffer from the rear module's feet being dragged on the ground while the front module's feet are striding. This dragging motion introduces an undesired friction force to the system that decreases the robot's translational velocity. **The optimum$_3$ gait of robot with compliant(T) backbones has a unique feet contact sequence where it lifts the rear module legs (R_3, L_3, R_4, and L_4) during the stride cycle of the other legs.** This lifting motion eliminates the undesired contact during the feet' opposing motion and removes the undesired friction forces. Additionally, the feet trajectories shown in figure 13(b) demonstrate the elimination of the slip motion. No-slip is another reason to obtain a higher velocity compared to the same robot operating with the continuous-trot gait.

Figures 12(c) and 13(c) show the optimum$_3$ gait diagram and the feet trajectory of the eight-legged four-module robot with rigid backbones. **Eight-legged four-module SMoLBot(R) running with the optimum$_3$ gait follows a similar locomotion behavior to the six-legged SMoLBot(R); such that the motion starts with striding on two feet and then falling on the third foot with a minimum number of contact points in an instant.**

Velocity results of the ten-legged five-module robots running with the continuous-trot gait and the optimum$_3$ gaits are shown in figure 14. Similar to the eight-legged and the six-legged robots, the ten-legged SMoLBot(I) have the highest increase in the velocity values while operating with the optimum$_3$ gait compared to the velocity of the robot operating with the continuous-trot gait. $\delta V = V_{\text{opt}} - V_{\text{trot}}$ for the ten-legged five-module robots with compliant(I), compliant(T), and rigid backbones are 25 mm(s)$^{-1}$, 20 mm(s)$^{-1}$, and 23 mm(s)$^{-1}$, respectively. Furthermore, the experimental velocities of the ten-legged five-module robots with compliant(I), compliant(T), and rigid backbones operating with optimum$_3$ gaits are 85 mm(s)$^{-1}$, 100 mm(s)$^{-1}$, and 105 mm(s)$^{-1}$, respectively (experimental velocities in body-length/s unit are as 0.45, 0.54, and 0.57). Table 4 shows the optimum feet phases of the ten-legged five-module robots with rigid, compliant(T) and compliant(I) backbones. Figure 15 **shows the gait diagrams of the ten-legged robots. The results presented in figure 15 and table 4 shows that the compliant backbone robots tend to move the legs of each module together causing consecutive bouncing of the modules.**

Figure 15(a) shows the locomotion pattern of a ten-legged five-module SMoLBot(I) operating with the optimum$_3$ gait, in a single gait cycle with the time step of $\delta t = 0.1$. Blue arrows in figure 15(a) represent the nominal contact forces and the tangential friction forces of the feet, while the feet and the ground are in-contact. Figure 15(b) shows the optimum$_3$ gait diagram of the ten-legged five-module robot with compliant(I) backbones. **Ten-legged five-module SMoLBot(I) operating with the optimum$_3$ gait uses only five periodically changing legs to stride. All modules of the ten-legged SMoLBot(I) have a lift and drop motion, in which, at some instant, both feet of the *i*th module lose contact with the ground. The module losing ground contact is periodically changing during the gait cycle. This lift motion reduces the slip length and increases the velocity by**

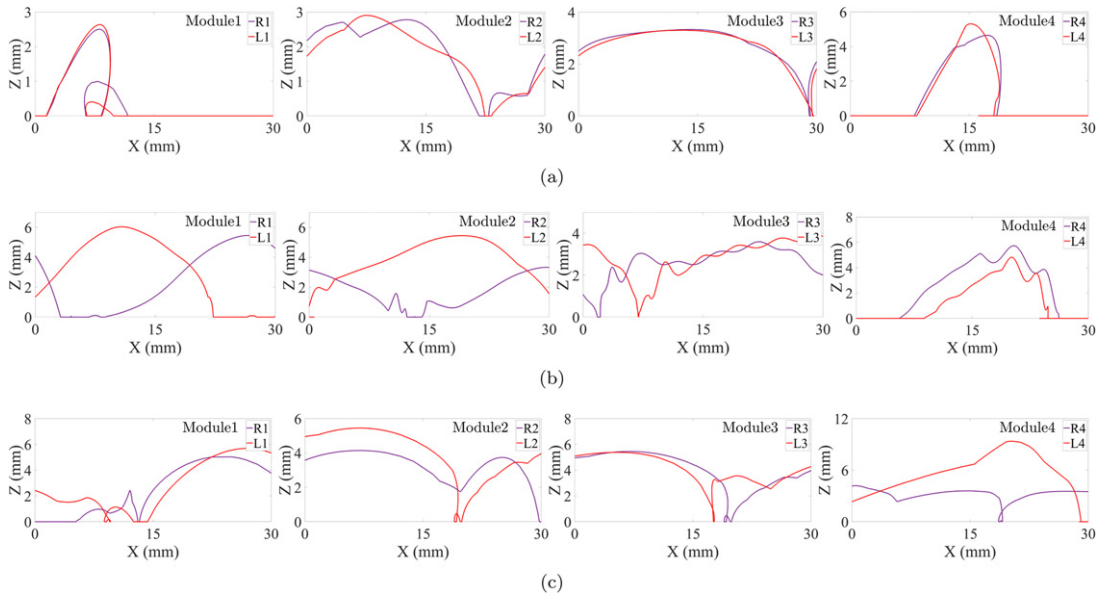

Figure 13. Feet trajectories of the eight-legged four-module robots operating with optimum$_3$ gaits in a single gait cycle with (a) compliant(I), (b) compliant(T), and (c) rigid backbones. The stepping frequency is chosen as 3 Hz.

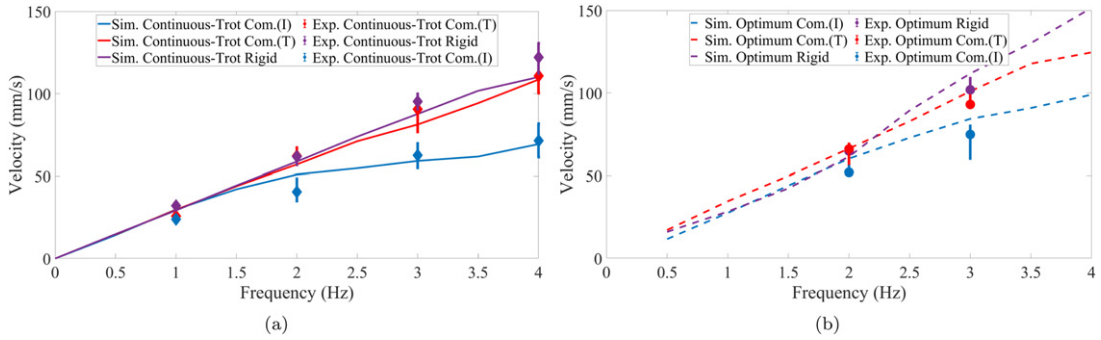

Figure 14. (a) Simulation and experimental velocity results of the ten-legged five-module robots with rigid, compliant(T) and compliant(I) backbones operating with (s) continuous-trot, and (b) optimum$_3$ gait.

eliminating the additional friction forces due to the feet' dragging and slipping.

Figure 15(c) shows the optimum$_3$ gait diagram of the ten-legged robot with compliant(T) backbones. **Ten-legged five-module SMoLBot(T) has a feet contact sequence where at any instant, only two pairs of right and left feet are in contact with the ground.** This generates statically stable locomotion with maximum contact during the stride period. Optimum$_3$ gait diagram of the ten-legged five-module robot with rigid backbones is shown in figure 15(d). **Ten-legged five-module SMoLBot(R) running with the optimum$_3$ gait strides with only two legs and then falls on a third leg.** The periodical motion of the ten-legged SMoLBot(R) starts with the lift of the two front modules (figure 15(e)-positive pitch), follows with zero pitch at which the front modules are dropped, and finally, the motion ends by lifting the rear modules (figure 15(e)-negative pitch).

Compliance between the modules and feet contact sequence are two main characteristics of the miniature robots that can be exploited to operate the robot at its limits. **Results indicate the existence of a unique set of feet phases for specific backbone compliance maximizing the robot's velocity.** Interestingly, this optimum gait is very different from what we usually utilize in similar robots, which is an extended form of the trot gait or the alternating-tripod gait. Furthermore, comparing the results of the multi-legged robots operating with different gaits shows similar locomotion, i.e. robots with different backbone types have different optimum gaits; however, they have a similar locomotion behavior to maximize the velocity. **Robots with compliant backbones tend to have a bouncy motion (lift, jump, and fall) with a large pitch; this motion eliminates the slip (e.g. feet trajectories of eight-legged four-module robots shown in figure 13 demonstrates the elimination of the slip). On the other hand, rigid-backbone**

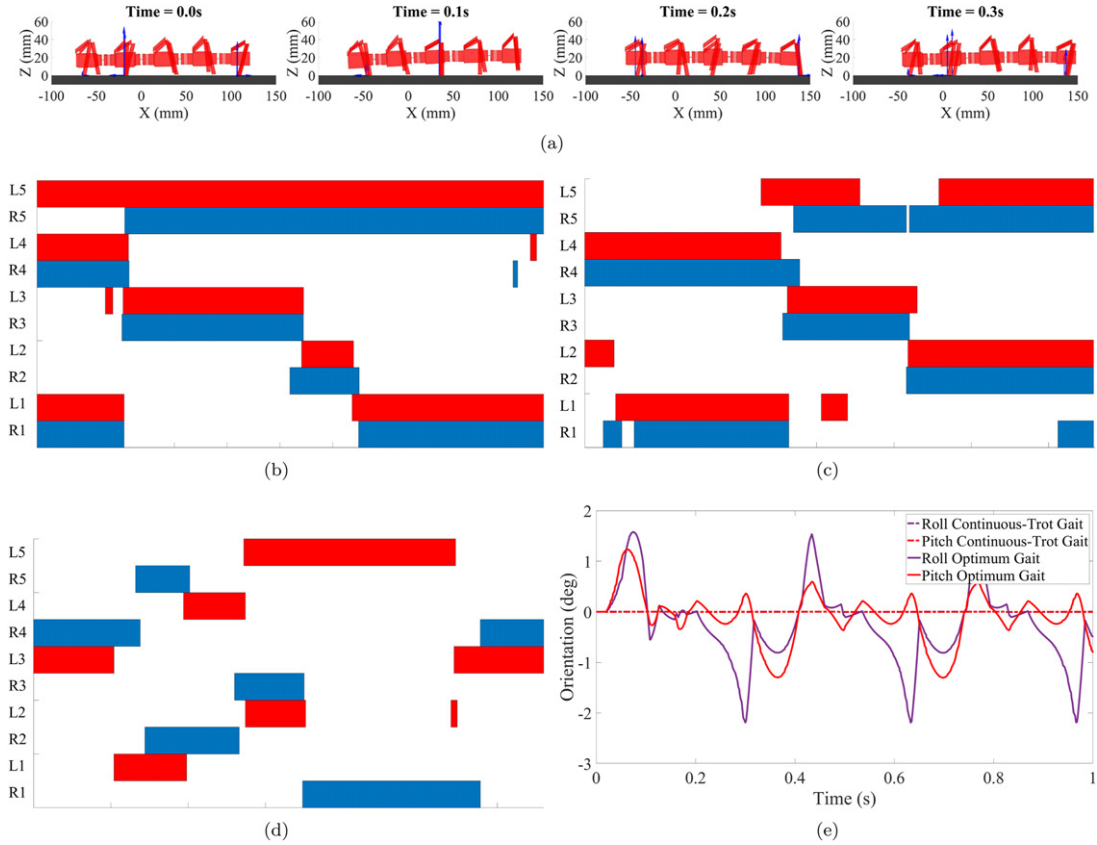

Figure 15. (a) Ten legged five-module SMoLBot(I)'s locomotion pattern in a single gait cycle with a $\delta t = 0.1$ time step operating with optimum$_3$ gait. Optimum$_3$ gait diagram of the ten-legged five-module (b) SMoLBot(I), (c) SMoLBot(T), and (d) SMoLBot(R). (e) Roll and pitch angles of the five-module SMoLBot(R) operating with the continuous-trot gait and the optimum$_3$ gait.

Table 4. Motor phases of the ten-legged five-module robot for optimum$_3$ gait.

	SMoLBot(I)	SMoLBot(T)	SMoLBot(R)
$R_1 - L_1$ (deg)	0–5	0–126	0–137
$R_2 - L_2$ (deg)	112–170	16–0	92–63
$R_3 - L_3$ (deg)	177–175	77–93	60–180
$R_4 - L_4$ (deg)	78–5	175–175	180–107
$R_5 - L_5$ (deg)	38–137	77–162	130–38

robots show a different type of locomotion behavior, such that they use a minimum number of rear or front feet to stride at any instant. This locomotion behavior results in a periodically switching motion of positive–negative pitch. Some of the simulations and experiments conducted for this work is combined into a multimedia attachment. The supplementary video demonstrates the bouncing motion of the robot more clearly.

5. Discussion

Gait mismatch of miniature robots introduces slipping and dragging motion into the system, decreasing the robot's translational velocity. However, the gait study presented here shows that running the robot at an optimum gait increases the robot's locomotion capabilities. Presented locomotion analyses in this manuscript indicate that uniquely obtaining an optimum gait for a specific set of design parameters (such as the backbone stiffnesses and a module number) and operational needs eliminates/decreases the slip and drag motion and helps the robot to run faster.

In this manuscript, the locomotion analyses are first obtained using the dynamic model; next, the results are verified using an actual modular robot with backbones possessing similar bending and torsional stiffnesses. We observed two main locomotion behaviors: rigid robots use the minimum number of instantaneous in-contact feet and lift the front and rear section of the robot periodically to increase the velocity. A periodic positive-negative pitch angle wave-form depicts this motion. On the other hand, soft-backbone robots use a lift and jump motion. Mid-modules are periodically lifted, with rear and front modules supporting this lifting motion, and both feet of the ith module lose ground contact concurrently. This lifting motion of the modules eliminates undesired slip and increases the velocity. The same locomotion study presented here can be applied to analyze any other under-actuated miniature robot with a soft or rigid body. Additionally, although the feet phases will differ for any other robot with different design parameters, like module dimensions, weight, and backbone type, we believe they

will have locomotion behaviors similar to those discussed in this paper (lift-jump-fall locomotion and minimum in-contact feet behavior). The results presented here give an insight into the effects of different design parameters on our robot's overall locomotion, which helps the researchers have a perspective about the locomotion of the multi-legged miniature robots with soft and rigid modular connections.

6. Conclusion and future work

In this paper, the locomotion of a running/walking multi-legged miniature robot with different body compliances has been considered. Rather than using predefined common known gaits of the multi-legged robots, the possible gaits maximizing the robot's translational velocity are investigated. This approach evaluates the dynamics of a multi-legged robot with soft or rigid connections while considering the miniature robot's limitations to obtain the possible optimum gaits. Using the locomotion analyses of the robots running with numerically derived gaits, we found that miniature robots walk with a bouncing gait that has a lift–jump–drop periodical sequence to maximize the velocity or use a contact sequence with only a limited number of instantaneous feet–ground contacts. Furthermore, we have shown the existence of unique gaits that maximize the speed for modular miniature robots. Additionally, we have shown that the gaits of different robots with soft or rigid backbones follow a common principle to improve the locomotion speed, the multi-legged miniature robots operating with the optimum gaits walk in a way to minimize the feet slip. Soft-backbone multi-legged robots favor a lift and drop motion, and the rigid-backbone robots take advantage of using a statically-stable gait with a minimum number of instantaneous in-contact feet that minimize the slip and drag motion effects. Our analyses provide an insight into the locomotion trends of the multi-legged miniature robots with a soft or rigid body and can be used by the researchers while manufacturing and working with miniature robots.

While there are many ways to extend the work presented here, the primary future work would be active control and actuation of the backbones during the operation for a better gait implementation. Similarly, active control on the backbones makes it possible to improve the robot's obstacle climbing capabilities and can provide a mechanism for faster locomotion on rough terrain. Additional investigations to predict and study the robot's locomotion on rough terrains can be conducted to evaluate the optimum gaits on rough terrains that improve the locomotion of the legged miniature robots in real-world environments.

Acknowledgments

The authors would like to thank members of Bilkent Miniature Robotics Laboratory for their invaluable assistance throughout this project. This work is funded by the Scientific and Technological Research Council of Turkey (TUBITAK), Grant No. 116E177.

Data availability statement

All data that support the findings (http://stacks.iop.org/BB/16/066009/mmedia) of this study are included within the article (and any supplementary files).

ORCID iDs

Nima Mahkam https://orcid.org/0000-0001-5450-4624
Onur Özcan https://orcid.org/0000-0002-3190-6433

References

[1] Ding X and Yang F 2016 Study on hexapod robot manipulation using legs *Robotica* **34** 468–81
[2] Onal C D and Rus D 2012 A modular approach to soft robots *4th IEEE RAS EMBS Int. Conf. Biomedical Robotics and Biomechatronics (BioRob)* (Piscataway, NJ: IEEE) pp 1038–45
[3] Song Y S and Sitti M 2007 Stride: a highly maneuverable and non-tethered water strider robot *Proc. 2007 IEEE Int. Conf. Robotics and Automation* (Piscataway, NJ: IEEE) pp 980–4
[4] Alexander R M 1980 Optimum walking techniques for quadrupeds and bipeds *J. Zool.* **192** 97–117
[5] Rus D and Tolley M T 2018 Design, fabrication and control of origami robots *Nat. Rev. Mater.* **3** 101
[6] Onal C D, Wood R J and Rus D 2011 Towards printable robotics: origami-inspired planar fabrication of three-dimensional mechanisms *IEEE Int. Conf. Robotics and Automation* (Piscataway, NJ: IEEE) pp 4608–13
[7] Karakadioglu C, Askari M R and Özcan O 2017 Design and operation of MinIAQ: An untethered foldable miniature quadruped with individually actuated legs *IEEE Int.Conf. Adv. Intell. Mechatronics (AIM'17)* (Munich, Germany) pp 247–52
[8] Whitesides G M 2018 Soft robotics *Angew. Chem., Int. Ed.* **57** 4258–73
[9] Brunete A, Ranganath A, Segovia S, de Frutos J P, Hernando M and Gambao E 2017 Current trends in reconfigurable modular robots design *Int. J. Adv. Robot. Syst.* **14** 1729881417710457
[10] Mahkam N, Bakir A and Özcan O 2020 Miniature modular legged robot with compliant backbones *IEEE Robot. Autom. Lett.* **5** 3923–30
[11] Kindermann T 2001 Behavior and adaptability of a six-legged walking system with highly distributed control *Adapt. Behav.* **9** 16–41
[12] Schilling M *et al* 2008 Local control mechanisms in six-legged walking *IEEE/RSJ Int. Conf. Intelligent Robots and Systems* (Piscataway, NJ: IEEE) pp 2655–60

[13] Ozcan O *et al* 2014 Powertrain selection for a biologically-inspired miniature quadruped robot *IEEE Int. Conf. Robotics and Automation (ICRA)* (Piscataway, NJ:IEEE) 2398–405
[14] Hoover A M, Steltz E and Fearing R S 2008 Roach: an autonomous 2.4 g crawling hexapod robot *IEEE/RSJ Int. Conf. Intelligent Robots and Systems* (Piscataway, NJ: IEEE) pp 26–33
[15] Kaln MAI *et al* 2020 Design, fabrication, and locomotion analysis of an untethered miniature soft quadruped, squad *IEEE Robot. Automat. Lett.* **5** 3854–60
[16] Nguyen C T *et al* 2014 A small biomimetic quadruped robot driven by multistacked dielectric elastomer actuators *Smart Mater. Struct.* **23** 065005
[17] Karydis K *et al* 2015 Navigation of miniature legged robots using a new template *23rd Mediterranean Conf. Control and Automation (MED)* (Piscataway, NJ: IEEE) pp 1112–7
[18] Saranli U, Buehler M and Koditschek D E 2001 RHex: a simple and highly mobile hexapod robot *Int. J. Robot. Res.* **20** 616–31
[19] Roy S S and Pratihar D K 2012 Effects of turning gait parameters on energy consumption and stability of a six-legged walking robot *Robot. Auton. Syst.* **60** 72–82
[20] Nagy Z *et al* 2008 Experimental investigation of magnetic self-assembly for swallowable modular robots *IEEE/RSJ Int. Conf. Intelligent Robots and Systems* (Piscataway, NJ: IEEE) pp 1915–20
[21] Wang W, Wang K and Zhang H 2009 Crawling gait realization of the mini-modular climbing caterpillar robot *Prog. Nat. Sci.* **19** 1821–9
[22] Caporale J D *et al* 2020 Coronal plane spine twisting composes shape to adjust the energy landscape for grounded reorientation *IEEE Int. Conf. Robotics and Automation (ICRA)* (Piscataway, NJ: IEEE) pp 8052–8
[23] Alexander R M 1984 The gaits of bipedal and quadrupedal animals *Int. J. Robot. Res.* **3** 49–59
[24] Pierre R S and Bergbreiter S 2016 Gait exploration of sub-2 g robots using magnetic actuation *IEEE Robot. Autom. Lett.* **2** 34–40
[25] Ahmed A, Henrey M, Bloch P, Gupta P, Panaitiu C, Naaykens D, Strbac S, Shannon L and Menon C 2013 A miniature legged hexapod robot controlled by a fpga *Int. J. Mech. Eng. Mechatron.* **1** 1–6
[26] Birkmeyer P, Peterson K and Dash F R S 2009 A dynamic 16 g hexapedal robot *IEEE/RSJ Int. Conf. Intelligent Robots and Systems* (Piscataway, NJ: IEEE) pp 2683–9
[27] Bohra M M and Emami M R 2014 An evolutionary approach to feline rover gait planning *IEEE Int. Conf. Robotics and Biomimetics (ROBIO 2014)* (Piscataway, NJ: IEEE) pp 767–72
[28] Wang W, Gu D and Xie G 2017 Autonomous optimization of swimming gait in a fish robot with multiple onboard sensors *IEEE Trans. Syst. Man Cybern.* **49** 891–903
[29] Heaston J R and Hong D W 2009 Design optimization of a novel tripedal locomotion robot through simulation and experiments for a single step dynamic gait 48094 pp 715–24
[30] Mahkam N and Özcan O 2021 A framework for dynamic modeling of legged modular miniature robots with soft backbones *Robot. Auton. Syst.* **144** 103841
[31] Karakadıoğlu Cem, Askari Mohammad and Askari A 2020 The effect of large deflections of joints on foldable miniature robot dynamicsc *J. Intell. Robot. Syst.: Theory Appl.* **100**
[32] Stengel R F 2015 *Flight Dynamics* (Princeton, NJ: Princeton University Press)
[33] Mastalli C *et al* 2016 Hierarchical planning of dynamic movements without scheduled contact sequences *IEEE Int. Conf. on Robotics and Automation (ICRA)* (Piscataway, NJ:IEEE) 4636–41
[34] Posa M, Cantu C and Tedrake R 2014 A direct method for trajectory optimization of rigid bodies through contact *Int. J. Robot. Res.* **33** 69–81
[35] Önol A Ö *et al* 2020 Tuning-free contact-implicit trajectory optimization *IEEE Int. Conf. Robotics and Automation (ICRA)* (Piscataway, NJ: IEEE) pp 1183–9
[36] Sivanandam S and Deepa S 2008 Genetic algorithm optimization problems *Introduction to Genetic Algorithms* (Berlin: Springer) pp 165–209
[37] Archer R R *et al* 2012 *An Introduction to Mechanics of Solids* (New York: McGraw-Hill)
[38] Baisch A T *et al* 2011 Hamr3: an autonomous 1.7 g ambulatory robot *IEEE/RSJ Int. Conf. Intelligent Robots and Systems* (Piscataway, NJ: IEEE) pp 5073–9
[39] Pullin A O, Kohut N J, Zarrouk D and Fearing R 2012 Dynamic turning of 13 cm robot comparing tail and differential drive *IEEE Int. Conf. Robotics and Automation* (Piscataway, NJ: IEEE) pp 5086–93